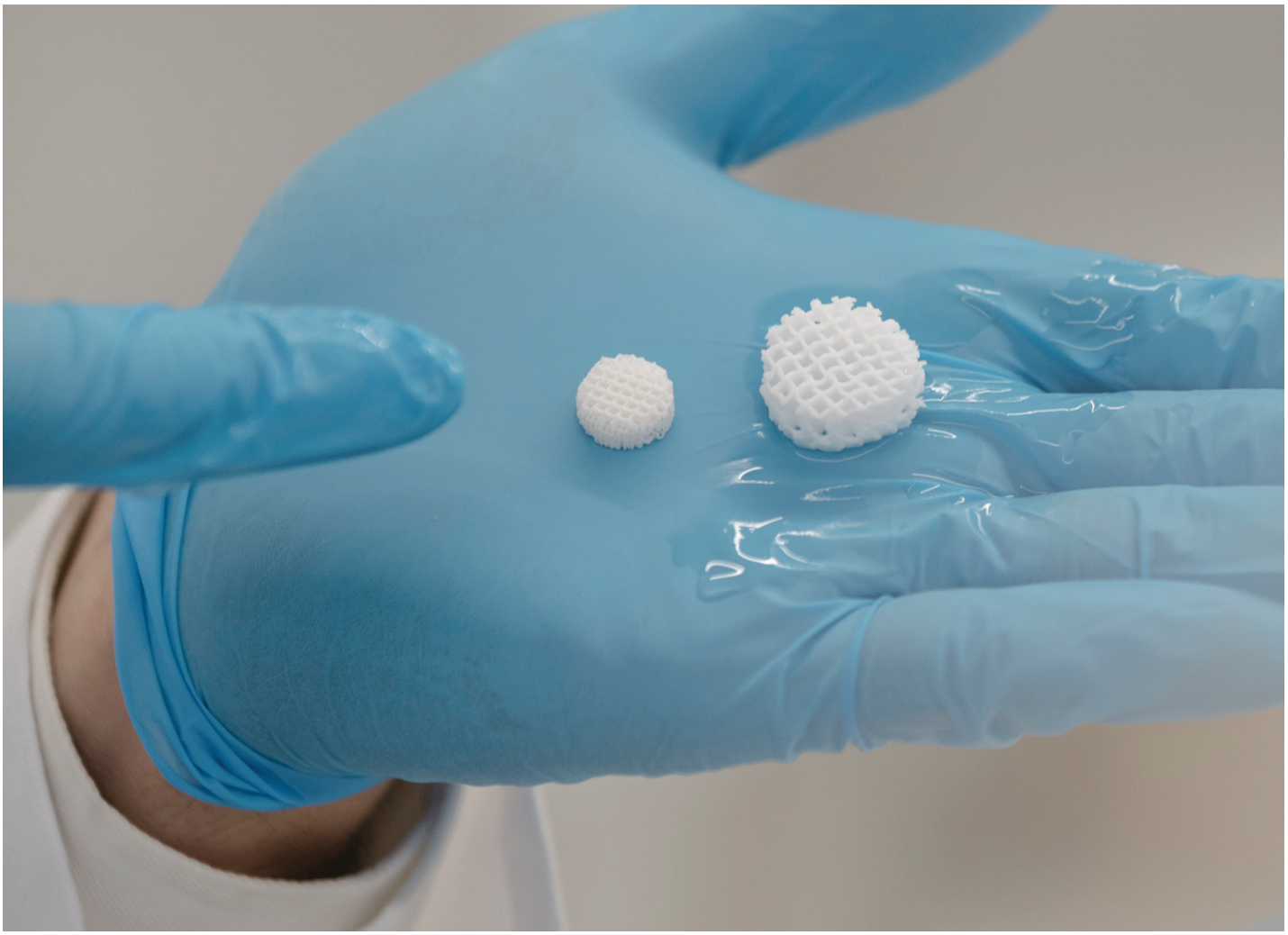

Showcasing research from Dr Aron Blaesi's group at Enzian Pharmaceutics, Zurich, Switzerland and Cambridge, MA, USA.

Enhancing the bioavailability of sparingly-soluble drugs by expandable, solid-solution fibrous dosage forms

At present, the effectiveness of many life-saving oral therapies employing a sparingly water-soluble drug is limited by the drug's bioavailability. For enhancing bioavailability, Blaesi's group at Enzian Pharmaceutics has developed an expandable, solid-solution fibrous dosage form. The fibrous form releases drug into the stomach at a high rate for prolonged time. In dogs it enhanced the bioavailability of the sparingly-soluble model drug nilotinib three-fold compared with the present crystalline drug particle-filled capsules.

Image reproduced by permission of Aron H Blaesi, Enzian Pharmaceutics Blaesi AG from *RSC Pharm.*, 2026, **3**, 88.

As featured in:

See Aron H. Blaesi *et al., RSC* Pharm., 2026, **3**, 88.

ROYAL SOCIETY OF CHEMISTRY

rsc.li/RSCPharma

Registered charity number: 207890

RSC Pharmaceutics

ROYAL SOCIETY OF CHEMISTRY

PAPER

View Article Online
View Journal | View Issue

Cite this: *RSC Pharm.*, 2026, **3**, 88

Enhancing the bioavailability of sparingly-soluble drugs by expandable, solid-solution fibrous dosage forms

Aron H. Blaesi, *[a,b] Henning Richter [c] and Nannaji Saka[d]

Many kinds of drug are sparingly soluble in the acidic gastric fluid, and are practically insoluble in the pH-neutral intestinal fluid. The efficacy of oral therapies employing such drugs is often limited by the amount of drug that can be delivered into the blood stream. For enhancing the amount delivered, in the present work an expandable, solid-solution fibrous dosage form is presented. The dosage form investigated was a cross-ply structure of fibers comprising 200 mg of the sparingly-soluble drug nilotinib molecularly dispersed in hydroxypropyl methylcellulose (HPMC)-based excipient. Upon administering to a dog, it expanded to a normalized radial expansion of 0.5 within an hour and resided in the stomach for about five hours. The drug concentration in blood rose to a maximum of 1.82 μg ml^{-1} by 4 hours, and decayed exponentially thereafter. The bioavailability (area under the drug concentration in blood *versus* time curve) was 10.81 μg h ml^{-1}. For comparison, the maximum drug concentration of an immediate-release capsule filled with 200 mg crystalline nilotinib particles was 0.68 μg ml^{-1} by 2.5 hours. The bioavailability was 2.94 μg h ml^{-1}, a third of that of the fibrous form. Models suggest that the greater bioavailability of the fibrous dosage form is due to increased gastric residence time and supersaturation of the gastric fluid with the drug.

Received 23rd July 2025,
Accepted 29th October 2025

DOI: 10.1039/d5pm00195a

rsc.li/RSCPharma

1. Introduction

At present, many kinds of drug are sparingly soluble in the acidic gastric fluid, and are virtually insoluble in pH-neutral intestinal fluid.[1–5] The efficacy of oral therapies employing such drugs is often limited by the drug's bioavailability, A, defined here as:

$$A = \int_0^\infty c_{d,b}(t)\mathrm{d}t \qquad (1)$$

where $c_{d,b}$ is the drug concentration in blood and t is the time after administering a dosage form.

More specifically, as shown schematically in Fig. 1a, the most prevalent oral dosage forms at present are loose or lightly compacted mixtures of crystalline drug and excipient particles.[5–7] Upon ingestion, they disintegrate into their constituents in the stomach, Fig. 1b. The drug particles then

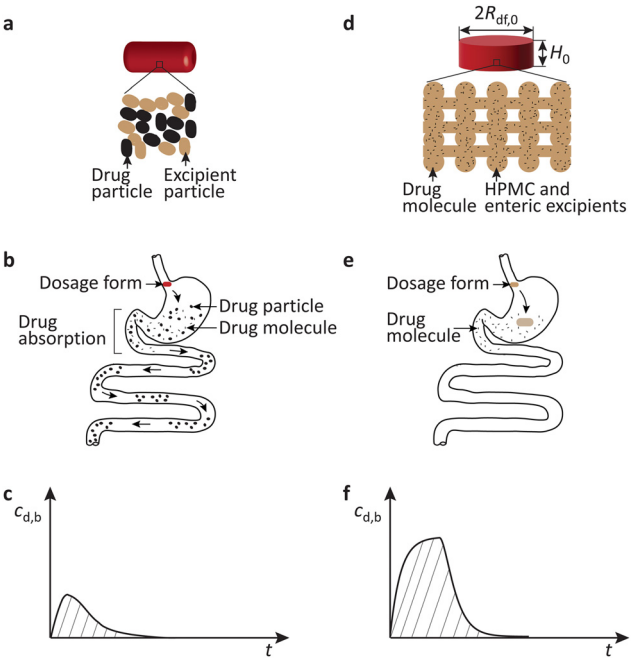

Fig. 1 Schematics of dosage form microstructure, passage through the gastrointestinal tract, and drug concentration in blood after single dosing: (a)–(c) particulate dosage form, and (d)–(f) solid-solution fibrous dosage form. $c_{d,b}$: drug concentration in blood; t: time. Bioavailability is the area under the curve.

[a]*Enzian Pharmaceutics Blaesi AG, CH-7078 Lenzerheide, Switzerland*
[b]*Enzian Pharmaceutics, Inc., Cambridge, MA 02139, USA.*
E-mail: ablaesi@enzianpharma.com
[c]*Diagnostic Imaging Research Unit (DIRU), Department of Clinical Diagnostics and Services, Vetsuisse Faculty, University of Zurich, CH-8057 Zurich, Switzerland*
[d]*Department of Mechanical Engineering, Massachusetts Institute of Technology, Cambridge, MA 02139, USA*

release drug molecules which pass into the intestine and are absorbed by the blood stream. As a result, the drug concentration in blood increases, Fig. 1c.

However, because the drug solubility in the gastric fluid is low, the drug particle dissolution rate is slow, and the drug concentration in blood increases slowly. Moreover, the small drug particles readily pass from the stomach into the intestine with the flowing gastric fluid. In the intestine they will not dissolve any further, Fig. 1b, and drug absorption stops. Thus, the drug concentration in blood peaks at a low value, the bioavailability is low, and the drug therapy may not be effective, Fig. 1c.

Over the years, therefore, numerous techniques have been developed to alter the physical state of sparingly-soluble drug particles. Such techniques include, for example, salt or co-crystal formation,[8,9] crystalline-to-amorphous phase transformation,[10–12] polymorphic change,[13,14] and formation of solid solutions.[15–20] While enhanced dissolution rates were achieved, the small drug particles still pass into the intestine prematurely.

Such limitations could be mitigated by the expandable fibrous dosage forms introduced recently.[21–28] As shown schematically in Fig. 1d, the fibrous dosage form considered here is a cross-ply structure of solid-solution fibers comprising dissolved drug molecules in a water-absorbing excipient matrix. Upon ingestion, the dosage form expands in the gastric fluid and releases drug molecules at a high rate. The expanded dosage form will not pass into the intestine instantly, and a high absorption rate can be maintained for prolonged time, Fig. 1e. This enhances the drug concentration in blood, bioavailability, and the efficacy of the drug therapy, Fig. 1f.

The specific solid-solution fibrous dosage forms investigated in the present work comprise 200 mg of the sparingly-soluble drug nilotinib dispersed in a matrix of hydroxypropyl methylcellulose (HPMC) and methacrylic acid–ethyl acrylate excipients. Dosage form expansion, drug release rate, gastric residence time, drug concentration in gastric fluid, drug concentration in blood, and bioavailability are determined by experiments and theoretical models. The dog is used as an animal model for *in vivo* studies.

The results are compared with those of a previously presented immediate-release capsule containing 200 mg crystalline nilotinib particles.[25–28] Details of the preparation, theoretical models, and properties of the particulate dosage forms are given in Appendix A.

2. Materials and methods

2.1. Materials of solid-solution fibrous dosage forms

The materials used for preparing the fibrous dosage forms were as follows.

(a) Drug. Nilotinib hydrochloride monohydrate, purchased as solid particles from either the European Directorate for the Quality of Medicine (EDQM), Strasbourg, France, or from Merck KGaA, Darmstadt, Germany.

(b) Excipients. Hydroxypropyl methylcellulose (HPMC) with a number-average molecular weight of 120 kg mol^{-1}, purchased from Merck KGaA, Darmstadt, Germany; methacrylic acid–ethyl acrylate copolymer (1 : 1), with a molecular weight of about 250 kg mol^{-1} (trade name: Eudragit L100-55), received from Evonik, Essen, Germany.

(c) Contrast agent. Barium sulfate ($BaSO_4$), purchased as solid particles of size ~1 μm, from Humco, Austin, TX.

(d) Solvent. Dimethylsulfoxide (DMSO), purchased from Merck KGaA, Darmstadt, Germany.

2.2. Preparation of solid-solution fibrous dosage forms

First, solid particles of nilotinib, HPMC, Eudragit L100-55, and $BaSO_4$ were mixed with liquid DMSO to form a uniform suspension. The concentrations of nilotinib, HPMC, Eudragit L100-55, and $BaSO_4$ were 105.2, 161.3, 53.8, and 137.3 mg ml^{-1} DMSO, respectively.

Then the suspension was extruded through a laboratory extruder to form a uniform viscous paste. The viscous paste was put in a syringe equipped with a hypodermic needle of inner radius, R_n = 205 μm. The paste was extruded through the needle to form wet fiber that was patterned layer-by-layer as a fibrous dosage form with cross-ply structure.[21–30] The nominal inter-fiber spacing, λ_n, in the patterned structure was 820 μm.

After patterning, to evaporate the solvent and solidify the structure the dosage forms were put in a vacuum chamber maintained at a pressure of 200 Pa and a temperature of about 35 °C for a day. The solid dosage forms then consisted of 23 wt% nilotinib, 35.25 wt% HPMC, 11.75 wt% Eudragit L100-55, and 30 wt% $BaSO_4$. They were 6.5 mm thick, and were trimmed to circular disks with nominal diameter 14 mm. The weight of the final, circular dosage forms was about 870 mg, and the weight of nilotinib in the dosage form was 200 mg, Table 1.

Table 1 Geometry, microstructural parameters, and composition of the solid-solution fibrous dosage forms

Symbol	Description	Value
H_0	Thickness of solid dosage form	6.5 mm
$M_{d,0}$	Mass of drug in dosage form	200 mg
M_{df}	Mass of the "final" dosage form	870 mg
n_l	Number of fiber layers in dosage form	32
$R_{df,0}$	Radius of dosage form	7 mm
$R_{f,0}$	Fiber radius	149 ± 7 μm[a]
w_{BaSO_4}	Weight fraction of $BaSO_4$ in fibers	0.3
w_d	Weight fraction of drug in fibers	0.23
w_{ee}	Weight fraction of enteric excipient (Eudragit L100-55) in fibers	0.1175
w_{HPMC}	Weight fraction of HPMC in fibers	0.3525
λ_0	Inter-fiber distance	601 ± 12 μm[a]
φ_f	Volume fraction of fibers in dosage form	0.57[b]

[a] From the scanning electron micrographs shown in Fig. 2. [b] From eqn (2) and (3).

2.3. Imaging the microstructures of the fibrous dosage forms

The microstructures of the fibrous dosage forms were imaged by a Zeiss Merlin High Resolution SEM with a GEMINI column. Top surfaces were imaged after coating with a 10 nm thick layer of gold. Longitudinal sections were imaged after cutting the dosage form with a thin blade (MX35 Ultra, Thermo Scientific, Waltham, MA) and coating with gold as above. All specimens were imaged with an in-lens secondary electron detector. The accelerating voltage was 5 kV, and the probe current 95 pA.

2.4. Differential scanning calorimetry (DSC)

DSC experiments were conducted on fibers of a fibrous dosage form after one year of storage at room temperature, and on the solid particles of nilotinib hydrochloride monohydrate used to prepare them. A sample of about 10 mg was placed in an aluminum pan, and the specific heat flow to increase the temperature from 30 to 300 °C was measured with a NETZSCH DSC 204F1 Phoenix. The rate of temperature rise was 10 °C per minute.

2.5. *In vitro* expansion of the fibrous dosage forms

The dosage forms were immersed in a beaker filled with 400 ml dissolution fluid (0.03 M HCl in DI water, pH = 1.5, at 37 °C). The fluid was stirred with a paddle rotating at 70 rpm. The immersed samples were then imaged periodically by a Nikon DX camera.

2.6. *In vitro* drug release by the dosage forms

Drug release by the dosage forms was determined by a USP dissolution apparatus II (Sotax AG, Aesch, Switzerland). The dissolution bath was filled with 1200 ml dissolution fluid (0.03 M HCl in DI water, pH = 1.5, at 37 °C). The fluid was stirred with a paddle rotating at 70 rpm. The dosage forms were immersed in the fluid, and the concentration of dissolved drug *versus* time was measured by UV absorption using a fiber optic probe connected to a Cary 60 UV-vis spectrophotometer (Agilent Technologies, Santa Clara, CA). Drug concentrations were determined by subtracting the UV absorbance at 310 nm wavelength from the absorbance at 300 nm.

2.7. *In vivo* gastric residence time of the dosage forms in dogs

For determining the gastric residence time of the fibrous dosage forms, two healthy beagle dogs (12.2 and 15.2 kg) were assigned an experiment each. The dogs fasted for 18 hours prior to the experiment.

The dosage forms were administered to an awake dog with 20 ml water as described previously.[23,28] Thereafter the dog was periodically placed in an X-ray permeable box, and the position of the dosage form in the gastrointestinal tract was monitored by biplanar fluoroscopy (using a Philips Allura Clarity fluoroscopy system). Between imaging, the dogs were allowed to roam about freely with access to water.

Five hours after administration, 180 grams of basic dry food was given (Grainfree 25/17, Petzeba AG, Alberswil, Switzerland). No sedatives, anesthesia, or other supplements were administered before, during, or after the experiment.

The study was conducted in compliance with the Swiss Animal Welfare Act (TSchG, 2005) and the Swiss Animal Welfare Ordinance (TSchV, 2008). It was approved by the Swiss Federal Veterinary Office Zurich; the animal license number was ZH072/2021.

2.8. Monitoring *in vivo* drug concentration in the blood of dogs

In addition to monitoring gastric residence, blood samples were periodically collected using a central venous catheter that was surgically inserted into the jugular vein of the dog at least 48 hours before the experiment. After collecting a sample, blood plasma was extracted. The nilotinib concentration in the plasma was measured by liquid chromatography coupled to tandem mass spectrometry (LC-MS/MS) as described previously.[28]

3. Results and discussion

3.1. Microstructures of solid-solution fibrous dosage forms

Fig. 2a and b are the top and sectional views of the fibrous dosage form. The fiber radius, $R_{f,0}$ = 149 μm, and the inter-fiber spacing, λ_0 = 601 μm, Table 1.

The volume fraction of fibers in the dosage form may be obtained by:[21–30]

$$\varphi_f = \xi \frac{\pi R_{f,0}}{2\lambda_0} \quad (2)$$

where ξ is the ratio of the "nominal" thickness of the dosage form (with point contacts at fiber crossings) and the "real" thickness of the dosage form (with flattened fiber-to-fiber contacts):

$$\xi = \frac{2R_{f,0}n_l}{H_0} \quad (3)$$

Here n_l is the number of stacked layers of fibers in the dosage form and H_0 the thickness of the solid dosage form. For the relevant parameter values ($R_{f,0}$ = 149 μm, λ_0 = 601 μm, n_l = 32, and H_0 = 6.5 mm), by eqn (2) and (3) φ_f = 0.57, Table 1.

3.2. Differential scanning calorimetry (DSC)

Fig. 3a presents the specific heat flow, q, into the fibers of the fibrous dosage form *versus* temperature, T. The heat flow was

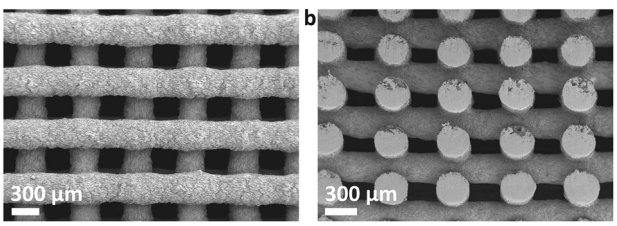

Fig. 2 Scanning electron micrographs of solid-solution fibrous dosage forms: (a) top view and (b) longitudinal section.

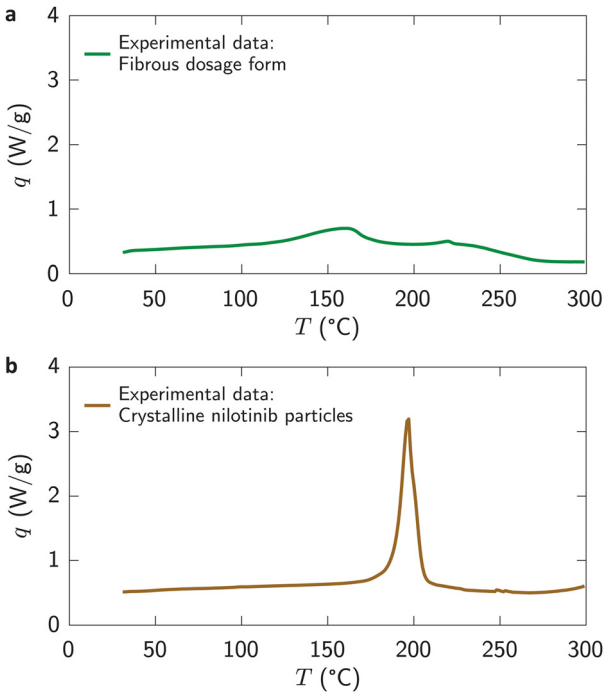

Fig. 3 Specific heat flow, q, *versus* temperature, T, into: (a) drug-laden fibers of a solid-solution fibrous dosage form and (b) the solid particles of nilotinib hydrochloride monohydrate used for preparing the fibrous dosage forms.

slightly greater than the baseline between 100 and 250 °C, and exhibited a broad peak at roughly 160 °C. However, no evidence of the presence of a crystalline nilotinib phase (*i.e.*, a sharp peak at ~200 °C, Fig. 3b) was found. Thus, the drug was molecularly dispersed in the excipient forming a solid solution.

3.3. *In vitro* expansion of fibrous dosage forms

Fig. 4 presents a sequence of top-view images of the fibrous dosage form after immersing in a stirred dissolution fluid. Fig. 5 in turn plots the normalized radial expansion, $\Delta R_{df}/R_{df,0}$, *versus* time, t. Initially, $\Delta R_{df}/R_{df,0}$ increased steeply, to 0.55 by 50 minutes. Thereafter it remained roughly constant.

As detailed in prior work,[21–23] the dosage forms expand due to the diffusion of water into the fibers. If the normalized radial expansion of the dosage form is assumed the same as the normalized radial expansion of a single fiber, an engineering approximation for $\Delta R_{df}/R_{df,0}$ may be written as:[21–23]

$$\frac{\Delta R_{df}}{R_{df,0}} \cong \frac{4}{3\sqrt{\pi}}\frac{c_b}{\rho_w}\left(\frac{D_w t}{{R_{f,0}}^2}\right)^{1/2} \quad (4)$$

where c_b is the boundary concentration of water in the fiber, ρ_w the water density, D_w the diffusivity of water in the fiber, and $R_{f,0}$ the initial fiber radius.

As shown in Fig. 5, up to 50 minutes the experimental data follow the curve $\Delta R_{df}/R_{df,0} = 0.0792t^{1/2}$. Substituting this result in eqn (4), and using $c_b/\rho_w = 1$ (Appendix B) and $R_{f,0} = 149$ μm, the diffusivity, $D_w = 4.1 \times 10^{-12}$ m^2 s^{-1}. This is of the order of the previously reported $D_w \sim 1 \times 10^{-11}$ m^2 s^{-1}.[22,23] Thus, the expansion mechanism of the present fibrous dosage forms is comparable to that of previously reported fibrous forms, and eqn (4) is reasonable.

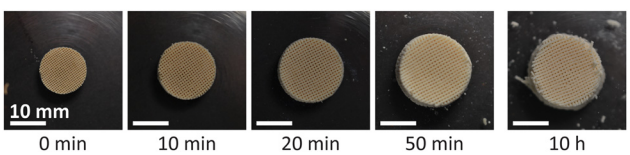

Fig. 4 Top-view images of a fibrous dosage form at various times after immersing in a dissolution fluid.

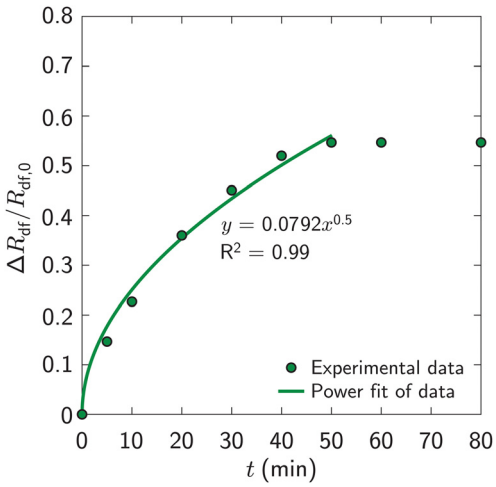

Fig. 5 Normalized radial expansion, $\Delta R_{df}/R_{df,0}$, of fibrous dosage form *versus* time, t, after immersing in the dissolution fluid. The data represent the sample shown in Fig. 4.

3.4. *In vitro* drug release

Fig. 6 plots the fraction of drug released, $m_{d,r}/M_{d,0}$, by the fibrous dosage forms into the *in vitro* dissolution fluid *versus* time, t. The dosage forms released 20, 40, 60, and 80 percent of the drug by 0.7, 1.8, 4.4, and 10.8 hours.

As shown schematically in Fig. 7, because the fibers of the dosage forms considered here are fairly tightly packed ($R_{f,0}/\lambda_0 = 0.25$ and $\varphi_f = 0.57$, Table 1), fluid flow through the inter-fiber space may be assumed small. Moreover, the expansion time, $t_e \sim 1$ h, is much smaller than the drug release time, $t_{dr} \sim 10$ h. Within the expansion time, however, the drug molecules readily diffuse out of the thin, water-penetrated fibers. Thus, for modeling drug release the "initial" dosage form may be considered an expanded composite slab with uniform drug concentration.

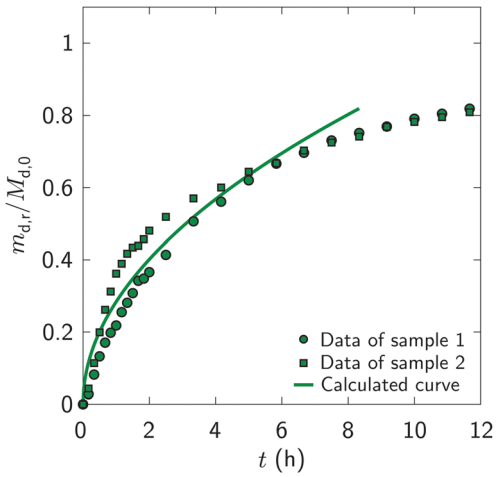

Fig. 6 Measured and calculated fraction of drug released, $m_{d,r}/M_{d,0}$, *versus* time, t, after immersing fibrous dosage forms in the dissolution fluid. The calculated curve is from eqn (8) using the parameter values of Appendix B. The data represent two samples.

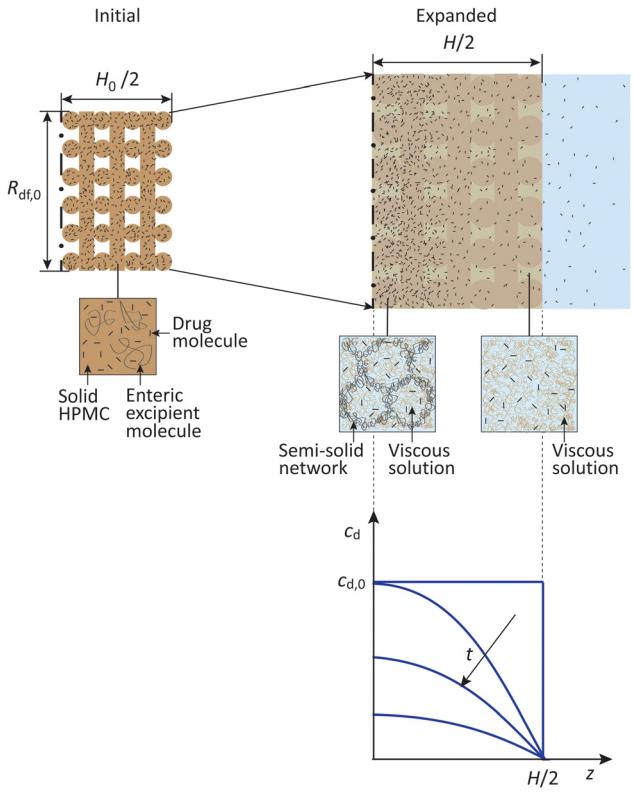

Fig. 7 Schematic microstructures of the initial and expanded dosage forms, and drug concentration profile in the expanded dosage form at various times. In the experiments, the radius and thickness of the initial dosage forms were: $R_{df,0}$ = 7 mm and H_0 = 6.5 mm. For illustrative purpose the drug molecules are shown in both the schematic microstructures of the fibrous dosage forms, and the enlargements of the fibers and the inter-fiber space.

The drug molecules then diffuse out of the slab, and the drug concentration decreases from the center of the slab to the surface. Assuming that the molecules do not precipitate and the geometry of the expanded dosage form is constant, for one-dimensional drug transport across the thickness, H, the diffusion equation may be written as:[31]

$$\frac{\partial c_d}{\partial t} = D_{d,df}\frac{\partial^2 c_d}{\partial z^2} \quad -H/2 \le z \le H/2 \tag{5a}$$

where c_d is the concentration and $D_{d,df}$ the diffusivity of drug molecules in the expanded dosage form.

The initial and boundary conditions are:

$$c_d = c_{d,0} \quad t = 0, \quad -H/2 < z < H/2 \tag{5b}$$

$$c_d = 0 \quad t \ge 0, \quad z = H/2 \tag{5c}$$

$$c_d = 0 \quad t \ge 0, \quad z = -H/2 \tag{5d}$$

where $c_{d,0}$ is the initial drug concentration in the expanded dosage form. Because the volume of the dissolution fluid is far greater than that of the dosage form and the fluid is stirred, the drug concentration in the fluid and at the surface of the dosage form may be considered zero.

The solution to eqn (5) may then be written as:[31]

$$\frac{c_d(r,t)}{c_{d,0}} = \frac{4}{\pi}\sum_{n=0}^{\infty}\frac{(-1)^n}{2n+1}\exp\left(-\frac{D_{d,df}(2n+1)^2\pi^2 t}{H^2}\right)\cos\left(\frac{(2n+1)\pi z}{H}\right) \tag{6}$$

By integrating eqn (6) over the volume of the dosage form and rearranging, the fraction of drug released may be obtained as:[31]

$$\frac{m_{d,r}(t)}{M_{d,0}} = 1 - \sum_{n=0}^{\infty}\frac{8}{(2n+1)^2\pi^2}\exp\left(-\frac{D_{d,df}(2n+1)^2\pi^2 t}{H^2}\right) \tag{7}$$

where $m_{d,r}(t)$ is the mass of drug released in time t and $M_{d,0}$ the initial drug mass in the fibrous dosage form.

For short times, eqn (7) may be approximated as:[31]

$$\frac{m_{d,r}(t)}{M_{d,0}} \simeq \frac{4}{\pi^{1/2}}\left(\frac{D_{d,df}t}{H^2}\right)^{1/2} \tag{8}$$

Fig. 6 also plots the calculated fraction of drug released by eqn (8) using $D_{d,df}$ = 4.22 × 10^{-10} m^2 s^{-1} and H = 9.8 mm (Appendix B). Up to seven hours ($m_{d,r}/M_{d,0} \sim 0.75$), the calculated fraction is comparable to the measured values. Thus, eqn (8) is reasonable; the drug is released in proportion to the square-root of time.

3.5. Gastric residence time

Fig. 8 presents fluoroscopic images of the position, shape, and size of a fibrous dosage form at various times after administering to a dog. The dosage form reached the stomach almost immediately, expanded, and formed a semi-solid mass. Initially, the normalized radial expansion, $\Delta R_{df}/R_{df,0}$, increased steadily with time, to 0.45 by 50 minutes. Thereafter, the dosage form was rounded off at the edges and $\Delta R_{df}/R_{df,0}$ decreased. By 330 minutes the remainder of the dosage form passed into the intestine and dissolved.

The average gastric residence time, $t_{r,f}$, of the two fibrous dosage forms tested was 5.5 h, Table 2. This value will be used in the models that follow.

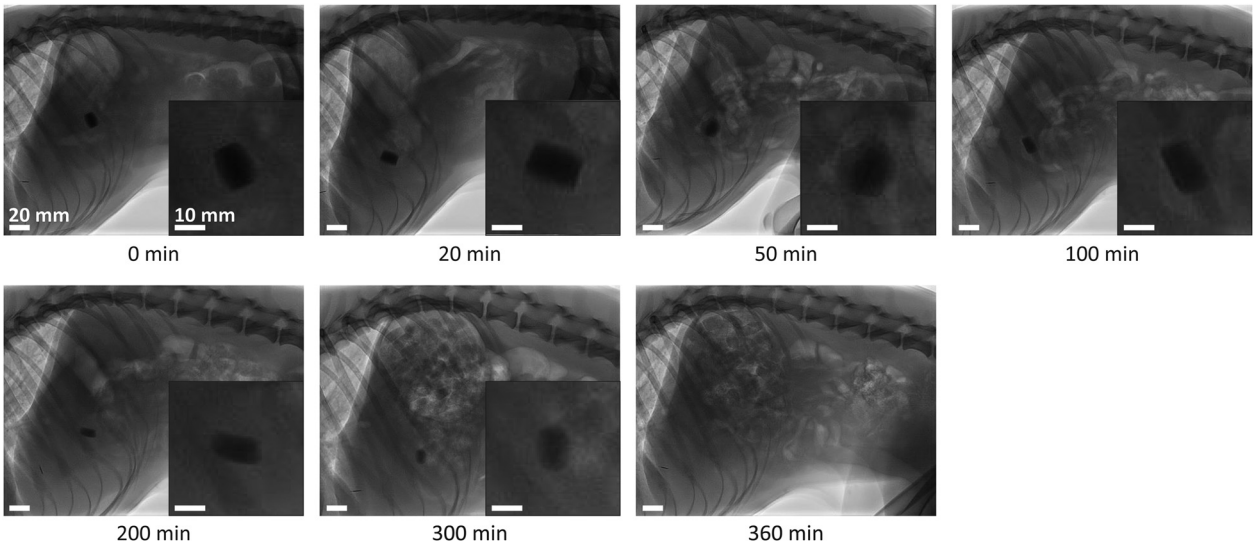

Fig. 8 Position and shape of a fibrous dosage form after administering to a dog after fasting. The first image (at 0 min) was taken almost immediately (*e.g.*, about a minute or less) after administering the dosage form. Dry food was given 5 hours after administration; it is visible in the images at 5 and 6 hours. The images were obtained by biplanar fluoroscopy. They show the abdomen in lateral projection (cranial left, caudal right).

Table 2 Measured and calculated quantities after administering fibrous and particulate dosage forms to dogs

		Fibrous dosage forms		Particulate dosage forms	
Quantity	Symbol and unit	Measured	Calculated	Measured	Calculated
In vitro					
Normalized radial expansion[a]	$\Delta R_{df}/R_{df,0}$ (—)	$0.614t^{1/2}$	—	—	—
Time to reach "terminal" expansion[a]	t_e (h)	0.83	—	—	—
"Terminal" normalized expansion[a]	$\Delta R_{df}/\Delta R_{df,0}\vert_{t=t_e}$ (—)	0.55	—	—	—
Time to release eighty percent of drug[b]	$t_{0.8}$ (h)	10.8	7.9	—	—
In vivo[c]					
Time to reach "terminal" expansion[d]	t_e (h)	0.83	—	—	—
"Terminal" normalized expansion[d]	$\Delta R_{df}/\Delta R_{df,0}\vert_{t=t_e}$ (—)	0.45	—	—	—
Gastric residence time[e]	$t_{r,f}$ and $t_{r,p}$ (h)	5.5	—	1–1.5	1.43
Time at which drug concentration in blood is maximal[f]	t_{max} (h)	4.0	4.3	2.5	2.2
Maximum drug concentration in blood[f]	c_{max} (μg ml^{-1})	1.82	1.2	0.68	0.59
Bioavailability[f]	A (μg h ml^{-1})	10.81	8.43	2.96	2.83

[a] The measured *in vitro* properties of $\Delta R_{df}/R_{df,0}$, t_e, and $\Delta R_{df}/R_{df,0}\vert_{t=t_e}$ are from Fig. 4 and 5. The unit of the time, t, is hours. [b] The measured $t_{0.8}$ of the fibrous dosage forms represents the average of two samples. The $t_{0.8}$ times of the individual samples were 10.5 and 11.1 hours, respectively, Fig. 6. The calculated $t_{0.8}$ is from eqn (8) using the parameter values of Appendix B. [c] The *in vivo* values represent averages of two fibrous and four particulate dosage forms. The mass of drug in all dosage forms was 200 mg. The masses of the dogs were 12.2 and 15.2 kg (fibrous dosage forms) and between 12.6 and 16.1 kg (particulate dosage forms). [d] Measured *in vivo* properties of t_e and $\Delta R_{df}/R_{df,0}\vert_{t=t_e}$ are from fluoroscopic images as shown in Fig. 8. [e] The gastric residence time of the individual fibrous dosage forms, $t_{r,f}$ = 6 and 5 h, respectively. The measured and calculated gastric residence times of the particulate forms, $t_{r,p}$, are from ref. 27 and 28 and recited in section A.3 of Appendix A. [f] The measured values of t_{max}, c_{max}, and A of the individual fibrous dosage forms were t_{max} = 4 h, c_{max} = 2.24 μg ml^{-1}, and A = 14.95 μg h ml^{-1} (sample 1), and t_{max} = 4 h, c_{max} = 1.41 μg ml^{-1}, and A = 6.68 μg h ml^{-1} (sample 2). The calculated values of t_{max}, c_{max}, and A of the fibrous dosage forms are from eqn (19), (21), and (22) using the parameter values of Appendix B. The measured and calculated values of t_{max} and c_{max} of the particulate dosage forms are from section A.5 of Appendix A.[27,28] The bioavailability, A, is from eqn (22) using the results and equations of section A.5 with the parameter values of Appendix B.

3.6. Drug concentration in gastric fluid

As will be shown later, the drug concentration in blood is directly dependent on the drug concentration in gastric fluid. Repeated collection of gastric fluid samples, however, is complex and beyond the scope of this work. Accordingly, the drug concentration in gastric fluid is estimated by mathematical models.

As shown schematically in Fig. 9, unlike the closed *in vitro* dissolution vessel, the stomach is an open system which is continuously filled by fresh gastric fluid (*i.e.*, fluid without any drug) and emptied by drug-containing fluid. The volume of the fasted stomach is small, and the mass of drug in the dosage form per unit volume of gastric fluid, $M_{d,0}/V_{gf} \gg c_{s,gf}$, the drug solubility (in this work, $M_{d,0}/V_{gf}$ = 10 mg ml^{-1} and $c_{s,gf}$ = 1 mg ml^{-1}, Appendix B).

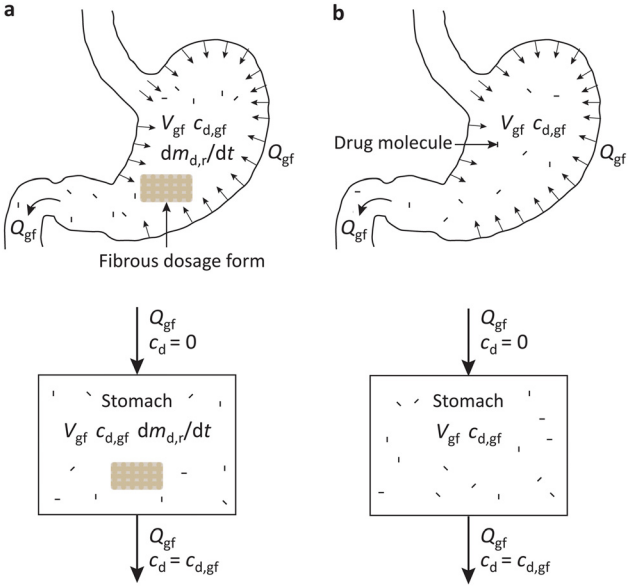

Fig. 9 Drug release in the stomach and drug transport from the stomach into the duodenum: (a) $0 \le t \le t_{r,f}$ and (b) $t > t_{r,f}$.

Assuming that: (a) the drug concentration in gastric fluid is uniform, (b) the drug does not precipitate in the gastric fluid, and (c) the flow rate of gastric fluid into the stomach is the same as the flow rate out, by mass balance the drug concentration in the gastric fluid may be written as:[27]

$$V_{gf}\frac{dc_{d,gf}}{dt} = -Q_{gf}c_{d,gf} + \frac{dm_{d,r}}{dt} \quad (9)$$

where V_{gf} is the volume of gastric fluid, Q_{gf} the volumetric flow rate of gastric fluid into and out of the stomach, and $dm_{d,r}/dt$ the drug release rate by the dosage form into the gastric fluid.

(a) $0 \le t \le t_{r,f}$. Up to the gastric residence time, $t_{r,f}$, the drug release rate may be obtained by differentiating eqn (8) and rearranging as:

$$\frac{dm_{d,r}(t)}{dt} = \frac{2M_{d,0}}{\pi^{1/2}}\left(\frac{D_{d,df}}{H^2 t}\right)^{1/2}. \quad (10)$$

For the parameter values listed in Appendix B, $M_{d,0}$ = 200 mg, $D_{d,df} = 4.22 \times 10^{-10}$ m^2 s^{-1}, and H = 9.8 mm, by eqn (9) $dm_{d,r}/dt$ = 50, 30, and 14 mg h^{-1} after 1, 3, and 5 hours, respectively. Thus, up to 5 hours the drug release rate from the dosage form is greater than the flow rate of drug out of the stomach at solubility, $Q_{gf}c_{s,gf}$ = 14 mg h^{-1}, Appendix B. Consequently, the gastric fluid may supersaturate with the drug.

Substituting eqn (10) in eqn (9) and rearranging gives:

$$\frac{dc_{d,gf}}{dt} + \frac{c_{d,gf}}{\tau_{gf}} = \alpha t^{-1/2} \quad (11a)$$

where

$$\tau_{gf} = \frac{V_{gf}}{Q_{gf}} \quad (11b)$$

$$\alpha = \frac{2M_{d,0}}{\pi^{1/2}V_{gf}}\left(\frac{D_{d,df}}{H^2}\right)^{1/2} \quad (11c)$$

Eqn (11a) is a first-order heterogeneous linear differential equation with positive and constant coefficients, and a source term that is a function of $t^{-1/2}$. To our knowledge, such a differential equation cannot be solved analytically. Thus, an approximate of eqn (11a) is written as a finite difference equation with time points, t_i, and time increment, Δt:

$$\frac{c_{d,gf}(t_{i+1}) - c_{d,gf}(t_i)}{\Delta t} + \frac{c_{d,gf}(t_{i+1})}{t_{gf}} = \alpha t_{i+1}^{-1/2} \quad (12a)$$

where

$$t_i = i\Delta t \quad i = 0, 1, 2, \ldots, \frac{t_{r,f}}{\Delta t} \quad (12b)$$

Rearranging eqn (11a), the drug concentration in gastric fluid at time t_{i+1} may be written as:

$$c_{d,gf}(t_{i+1}) = \frac{\Delta t\tau_{gf}}{\Delta t + \tau_{gf}}\left(\frac{c_{d,gf}(t_i)}{\Delta t} + \frac{\alpha}{t_{i+1}^{1/2}}\right) \quad i = 0, 1, 2, \ldots, \frac{t_{r,f}}{\Delta t} \quad (13)$$

Fig. 10a plots eqn (13) for the condition, $c_{d,gf}$ = 0 at t = 0, and the relevant parameter values listed in Appendix B. The drug concentration in gastric fluid rises rapidly to a maximum, c_{max} = 1.57 mg ml^{-1} (1.57 times the solubility) by t_{max} = 1.6 hours. Then it drops slowly to 1.03 mg ml^{-1} by the gastric residence time, $t_{r,f}$ = 5.5 hours.

(b) $t > t_{r,f}$. After the gastric residence time, no drug is released into the gastric fluid. Thus,

$$\frac{dm_{d,r}(t)}{dt} = 0 \quad (14)$$

Substituting eqn (14) in eqn (9) and rearranging gives:

$$\frac{dc_{d,gf}}{dt} + \frac{c_{d,gf}}{\tau_{gf}} = 0 \quad (15)$$

where the time constant, $\tau_{gf} = V_{gf}/Q_{gf}$.

Solving eqn (15) gives:

$$c_{d,gf} = c_{d,gf}\big|_{t=t_{r,f}} \exp\left(-\frac{t - t_{r,f}}{\tau_{gf}}\right) \quad (16)$$

where $c_{d,gf}\big|_{t=t_{r,f}}$ may be obtained from eqn (13).

Fig. 10a also plots eqn (16) for the relevant parameter values listed in Appendix B. After the residence time of the fibrous dosage form (at 5.5 hours) the drug concentration in gastric fluid drops exponentially at the time constant, τ_{gf} = 1.43 hours.

For comparison, as shown in Appendix A and plotted in Fig. 10a, after administering the crystalline particle-filled immediate-release capsule with the same drug content the drug concentration in gastric fluid drops already after about 1.5 hours and does not supersaturate. The calculated mass of drug dissolved in the gastric fluid $\left(= \int_0^\infty Q_{gf}c_{d,gf}\,dt\right)$ is 2.98 times smaller than that of the fibrous dosage form.

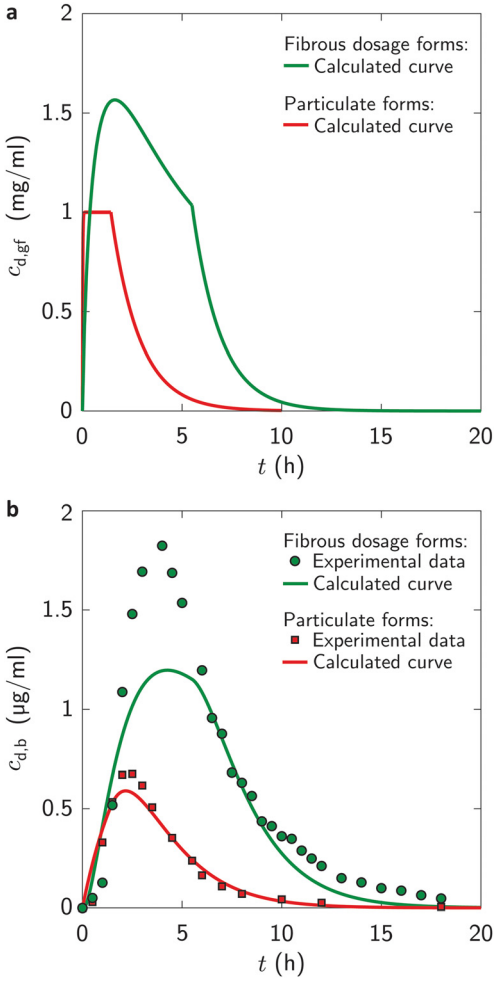

Fig. 10 (a) Calculated drug concentration in gastric fluid *versus* time after administering solid-solution fibrous and particulate dosage forms. The curve of the fibrous dosage form is from eqn (13) and (16) using the parameter values of Appendix B. The curve of the particulate form is from eqn (A3) and (A4) of Appendix A using the parameter values of Appendix B. (b) Measured and calculated drug concentrations in blood *versus* time. The measured values of the fibrous dosage forms represent the average drug concentration in blood plasma of two samples. Data of the individual samples are shown in Appendix C. Calculated values are from eqn (19) and (21) using the parameter values of Appendix B. Measured and calculated values of particulate dosage forms are reused from ref. 27 and 28 and recited in section A.5 of Appendix A.

3.7. Drug concentration in blood of dogs *versus* time

Fig. 10b plots the measured drug concentration in blood plasma *versus* time after administering the fibrous dosage forms. Initially, the concentration remained small for about an hour, but then it increased at a high rate to a maximum of 1.82 μg ml^{-1} by 4 hours. Past the maximum it decreased to 1.2 μg ml^{-1} by 6 hours, 0.21 μg ml^{-1} by 12 hours, and essentially zero by 18 hours.

The course of the drug after administering a fibrous dosage form is shown schematically in Fig. 11. It is assumed that (a) all drug molecules that are released into the stomach pass into the duodenum and are absorbed by

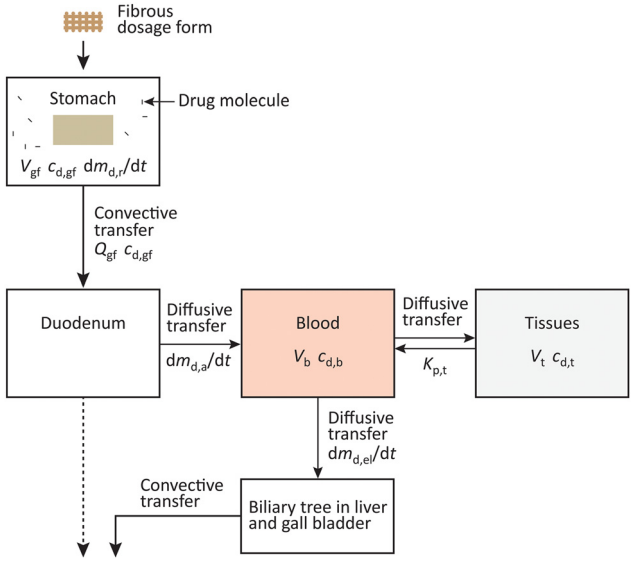

Fig. 11 Block diagram of drug release, absorption by the blood, inter-diffusion with tissues, and elimination. The absorption rate, $dm_a/dt = Q_{gf}c_{d,gf}$, and the elimination rate, $dm_{el}/dt = (V_b + K_{p,t}V_t)c_{d,b}/\tau_{el}$.[27]

the blood stream, (b) drug distribution through the blood and tissues is fast, and (c) the drug is eliminated from the blood at a rate proportional to the drug concentration in blood.

By mass balance the drug concentration in blood may then be written as:[27]

$$(V_b + K_{p,t}V_t)\frac{dc_{d,b}}{dt} = Q_{gf}c_{d,gf} - \frac{(V_b + K_{p,t}V_t)c_{d,b}}{\tau_{el}} \quad (17)$$

where V_b is the volume of blood, $K_{p,t} = c_{d,t}/c_{d,b}$ the tissue-blood partition coefficient of the drug ($c_{d,t}$ is the drug concentration in tissues), V_t the volume of tissues, and τ_{el} the time constant of the process by which drug is eliminated from the blood.

Eqn (17) shows that the drug concentration in blood is a function of the drug concentration in gastric fluid, $c_{d,gf}$, which in turn depends on the gastric residence time of the dosage form, $t_{r,f}$.

(a) $0 \le t \le t_{r,f}$. Substituting eqn (13) in eqn (17) and rearranging gives:

$$\frac{c_{d,b}(t_{i+1}) - c_{d,b}(t_i)}{\Delta t} + \frac{c_{d,b}(t_i)}{t_{el}} = \left(\frac{Q_{gf}}{V_b + K_{p,t}V_t}\right)c_{d,gf}(t_i) \quad (18)$$
$$i = 0, 1, 2, \ldots, \frac{t_r}{\Delta t}$$

Further rearranging:

$$c_{d,b}(t_{i+1}) = \left(1 - \frac{\Delta t}{t_{el}}\right)c_{d,b}(t_i) + \left(\frac{Q_{gf}\Delta t}{V_b + K_{p,t}V_t}\right)c_{d,gf}(t_i) \quad (19)$$
$$i = 0, 1, 2, \ldots, \frac{t_r}{\Delta t}$$

Eqn (19) provides a model for estimating the drug concentration in the whole blood comprising both blood cells and

plasma. If it is assumed that the partition coefficient between blood cells and plasma is unity, the drug concentrations in the blood (as modeled) and in the plasma (as measured) are the same.

Fig. 10b plots eqn (19) for the condition, $c_{d,b} = 0$ at $t = 0$, and the parameter values listed in Appendix B. The calculated drug concentration rises to a maximum, $c_{max} = 1.2$ μg ml^{-1} by $t_{max} = 4.3$ h, Table 2, and then drops. The calculated c_{max} is about 34 percent smaller than the measured value, and the calculated t_{max} is about the same.

The measured c_{max} may be greater because in the experiments the dosage form was rounded off in the stomach, and thus drug was released faster than predicted by eqn (8). Nonetheless, the agreement between model and data is fair.

(b) $t > t_{r,f}$**.** After the gastric residence time, the drug concentration in blood may be obtained by substituting eqn (16) in eqn (17) and rearranging as:

$$\frac{dc_{d,b}}{dt} + \frac{c_{d,b}}{\tau_{el}} = \frac{Q_{gf} c_{d,gf}\big|_{t=t_{r,f}}}{V_b + K_{p,t} V_t} \exp\left(-\frac{t - t_{r,f}}{\tau_{gf}}\right) \tag{20}$$

Solving gives:

$$c_{d,b} = c_{d,b}\big|_{t=t_{r,f}} \exp\left(-\frac{t - t_{r,f}}{\tau_{el}}\right) + \left(\frac{Q_{gf} c_{d,gf}\big|_{t=t_{r,f}}}{(V_b + K_{p,t} V_t)}\right)\left(\frac{\tau_{gf}\tau_{el}}{\tau_{el} - \tau_{gf}}\right)\left(\exp\left(-\frac{t - t_{r,f}}{\tau_{el}}\right) - \exp\left(-\frac{t - t_{r,f}}{\tau_{gf}}\right)\right) \tag{21}$$

where $c_{d,b}\big|_{t=t_{r,f}}$ may be obtained from eqn (19).

Eqn (21) is plotted in Fig. 10b for the parameter values listed in Appendix B. The calculated curve decays at about the same rate as the measured values.

For comparison, the measured and calculated drug concentrations in blood after administering the immediate-release capsules containing 200 mg crystalline nilotinib particles are also plotted in Fig. 10b. The measured and calculated c_{max} were 0.68 μg ml^{-1} by 2.5 hours and 0.59 μg ml^{-1} by 2.2 hours, respectively, Table 2.

Thus, as detailed in Appendix A, because the crystalline drug particles do not supersaturate the gastric fluid and the gastric residence time of the small particles is short, the drug concentration in blood increases at a lower rate and for a shorter time.

3.8. Bioavailability

Finally, by numerically integrating the integral in eqn (1), the bioavailability may be written as:

$$A = \sum_{i=1}^{n} \frac{c_{d,b}(t_i) + c_{d,b}(t_{i+1})}{2}(t_{i+1} - t_i) \tag{22}$$

where n is the number of data points of an experimental run (if $c_{d,b}$ was obtained from experiments) or the number of time points for which $c_{d,b}$ was calculated (if $c_{d,b}$ was obtained from numerical calculations).

Substituting the measured and calculated drug concentrations in the blood after administering the fibrous dosage forms, the measured and calculated bioavailabilities, 10.81 and 8.43 μg h ml^{-1}, respectively, Table 2.

For comparison, the measured and calculated bioavailabilities of the particulate dosage forms with crystalline drug particles are only 2.96 and 2.83 μg h ml^{-1}.

Thus, the solid-solution fibrous dosage forms enable enhanced bioavailablity compared with that of particulate dosage forms—in the present work by a factor three.

4. Conclusions

In this work, bioavailability of expandable, solid-solution fibrous dosage forms was investigated. The fibrous dosage forms were a cross-ply arrangement of fibers comprising 200 mg nilotinib molecularly dispersed in HPMC and methacrylic acid–ethyl acrylate excipients.

(a) ***In vitro*** **expansion of fibrous dosage forms.**

Upon immersing in a dissolution fluid, the fibrous dosage form expanded to 1.5 times the initial radius in 50 minutes. Models suggest that the normalized radial expansion of the dosage form initially scales as $(D_w t)^{1/2}/R_{f,0}$. Thus, the expansion was fast because the fibers were thin.

(b) ***In vitro*** **drug release.**

In the experiments, the dosage form released 20, 40, 60, and 80 percent of the drug by 0.7, 1.8, 4.4, and 10.8 hours. The modeled fraction of drug released scales as $(D_{d,df} t)^{1/2}/H$. Thus, because the expanded dosage form was thick, drug was released over prolonged time.

(c) Gastric residence time.

Upon administering to a dog, the fibrous dosage forms remained in the stomach for about 5.5 hours, and then passed into the intestine and dissolved.

(d) Drug concentration in gastric fluid.

Models suggest that during gastric residence the drug release rate by the fibrous dosage form into the gastric fluid, $dm_{d,r}/dt > Q_{gf} c_{s,gf}$, the mass flow rate of drug out of the stomach at solubility. Thus, the gastric fluid may supersaturate with the drug. After the gastric residence time, the drug concentration in gastric fluid falls exponentially.

(e) Drug concentration in the blood of dogs and bioavailability.

In the experiments, the drug concentration in blood rose to a maximum of 1.82 μg ml^{-1} by 4 hours and then decreased. The bioavailability (area under the drug concentration-time curve) was 10.81 μg h ml^{-1}. The data were reasonably close to the calculated values.

(f) Gastric residence time and drug concentration in gastric fluid of immediate-release particulate dosage forms.

By comparison, the modeled "gastric residence time" of small, sparingly soluble drug particles, $t_{r,p} = V_{gf}/Q_{gf} = 1.43$ hours, much shorter than that of the fibrous forms. Moreover, the drug release rate by crystalline drug particles, $dm_{d,r}/dt \sim (c_{s,gf} - c_{d,gf})$. Thus, the gastric fluid does not supersaturate. Due to both limitations the calculated mass of nilotinib dissolved in the gastric fluid is 3 times smaller than that of the fibrous dosage forms.

(g) Drug concentration in blood and bioavailability of particulate dosage forms.

Not surprisingly, therefore, after administering an immediate-release capsule filled with 200 mg crystalline nilotinib particles the maximum drug concentration was just 0.68 μg ml^{-1} by 2.5 hours. The bioavailability was only 2.96 μg h ml^{-1}.

It may be concluded, therefore, that due to the longer gastric residence time and supersaturation of the gastric fluid, the solid-solution fibrous dosage forms enhance the bioavailability of sparingly-soluble drugs. In the present work, the bioavailabiliy was enhanced by a factor of three.

Author contributions

Aron H. Blaesi: Development of dosage forms (conceptualization); production of dosage forms (resources); design and execution of *in vitro* experiments (methodology and investigation); design and assistance with *in vivo* experiments (methodology and investigation); data analysis (formal analysis); development of theory (methodology and investigation); writing (draft and editing). Henning Richter: Design and execution of *in vivo* experiments (methodology and investigation). Nannaji Saka: Data analysis (formal analysis); development of theory (methodology and investigation); writing (editing). All authors accepted the final manuscript for publication.

Conflicts of interest

AHB owns shares of Enzian Pharmaceutics. AHB and NS have filed for patents related to the technology presented in this manuscript. HR declares no competing interests.

Abbreviations

A	Bioavailability (area under drug concentration-time curve in units μg h ml^{-1})
c_b	Concentration of water at fiber–fluid interface
c_d	Drug concentration
$c_{d,0}$	"Initial" drug concentration in expanded dosage form
$c_{d,b}$	Drug concentration in blood or blood plasma
$c_{d,gf}$	Drug concentration in gastric fluid
c_{max}	Maximum drug concentration in blood
$c_{s,gf}$	Drug solubility in gastric or dissolution fluid
$D_{d,df}$	Diffusivity of drug through dosage form
$D_{d,fl}$	Diffusivity of drug in dissolution fluid
D_w	Diffusivity of water in fiber
H	Thickness of expanded dosage form
H_0	Thickness of solid dosage form
i	Integer index
$K_{p,t}$	Tissue-blood partition coefficient of drug
$M_{d,0}$	Mass of drug in dosage form
$m_{d,r}$	Mass of drug released
$m_{d,r}/M_{d,0}$	Fraction of drug released
$dm_{d,r}/dt$	Drug release rate
n	Number of time points
n_l	Number of stacked layers in dosage form
$n_{p,0}$	Number of drug particles in capsule
$n_{p,gf}$	Number of drug particles in gastric fluid
Q_{gf}	Flow rate of gastric fluid into the duodenum
q	Heat flow
R_{df}	Radius of expanding/expanded dosage form
$R_{df,0}$	Radius of solid dosage form
$R_{f,0}$	Radius of solid fiber
T	Temperature
t	Time
t_i	Time at index i
t_{max}	Time to reach maximum drug concentration in blood
$t_{r,f}$, $t_{r,p}$	Gastric residence time of fibrous and particulate dosage forms
$t_{0.8}$	Time to release 80 percent of drug content in a large-volume dissolution fluid
Δt	Time increment between integer indexes
V_b	Volume of blood
V_{gf}	Volume of gastric fluid
V_t	Volume of organs and tissues
x, y, z	Cartesian coordinates
α	Dimensional constant
β	Dimensional constant
λ_0	Inter-fiber distance in solid dosage form
ξ	Dimensionless constant
ρ_w	Density of dissolution fluid (acidic water)
τ_{el}, τ_{gf}	Time constants
φ_f	Volume fraction of fibers in dosage form

Data availability

The data that support the findings of this study are presented in the manuscript.

Appendix

A: Preparation and properties of particulate dosage forms

In this appendix, the previous studies on immediate-release particulate dosage forms[26,28] are reviewed and augmented by differential scanning calorigrams.

A.1. Preparation and microstructure. The particulate dosage forms were prepared as follows.[26,28] First, the contents of a

marketed immediate-release capsule containing 200 mg nilotinib particles and 200 mg of particulate excipients (trade name: Tasigna; purchased from Novartis, Basel, Switzerland) were removed. Then 170 mg of the contrast agent $BaSO_4$ (purchased as solid particles from Humco, Austin, TX) were mixed with the contents. Finally, an empty capsule of size 00 (trade name: Interdelta; purchased from Capsugel, La Seyne sur Mer, France) was filled with the mixture and closed.

Fig. 12 is a scanning electron micrograph of drug and excipient particles of the dosage form prior to mixing with the contrast agent.[26,28] The average particle radius was about 18.5 μm.

A.2. Differential scanning calorimetry (DSC). About 10 mg of drug and excipient particles were loaded in an aluminum pan and the specific heat flow to increase the temperature from 30 to 300 °C was measured with a NETZSCH DSC 204F1 Phoenix. The rate of temperature rise was 10 °C per minute.

Fig. 13 plots the specific heat flow, q, into the drug and excipient particles *versus* temperature. The heat flow exhibited narrow peaks at 147, 169, and 204 °C. Fig. 3b and prior work[32] suggest that the peak at 204 °C represents phase transformation of nilotinib from crystalline to a melt. Thus, the drug particles in the particulate dosage forms were in crystalline form.

A.3. Gastric residence time of particulate dosage forms. Fig. 14 presents fluoroscopic images of the position, shape, and size of the particle-filled capsule after administering to a fasted dog. Initially, the capsule was unbroken in the stomach. But after two minutes, it was fragmented and released contrast agent into the gastric fluid. By six minutes, the capsule was essentially disintegrated. Residual contrast agent was seen in the stomach up to 60–90 minutes after ingestion.

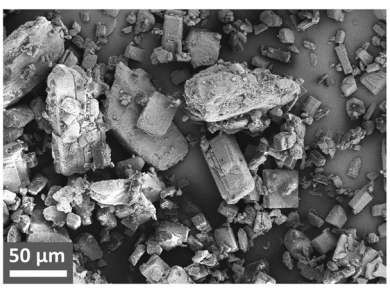

Fig. 12 Scanning electron micrograph of drug and excipient particles of the previously presented particulate dosage form. The image is reused from ref. 26.

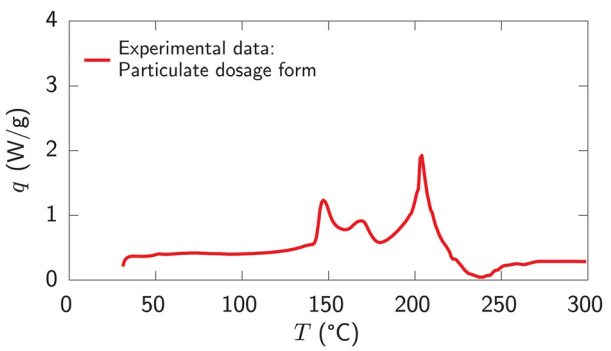

Fig. 13 Specific heat flow, q, into the drug and excipient particles of a particulate dosage form (without contrast agent) *versus* temperature, T.

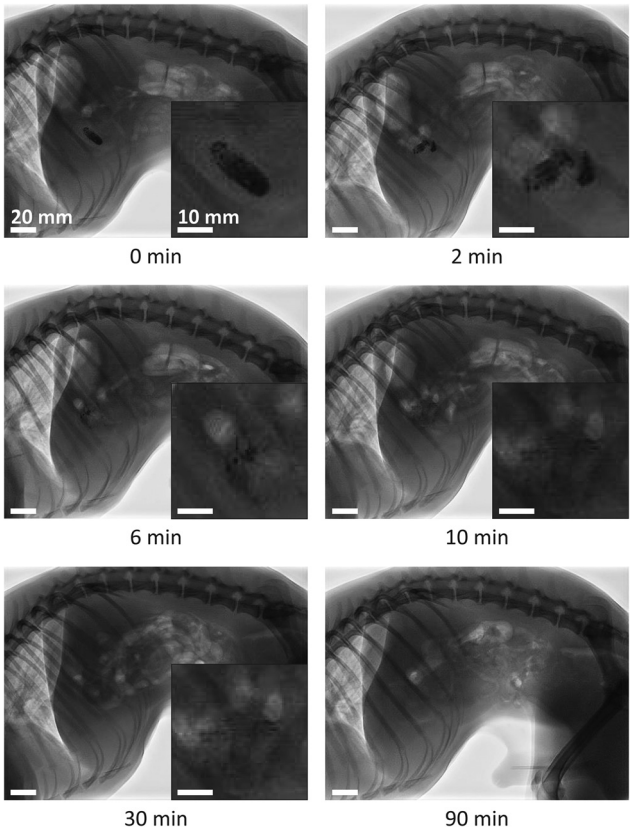

Fig. 14 Position and shape of a particulate dosage form administered to a fasted dog. The images were obtained by biplanar fluoroscopy. They show the abdomen in lateral projection (cranial left, caudal right). The images are reused from ref. 28.

As detailed in prior work[27,28] and Fig. 15, upon entering the stomach the particle-filled capsule disintegrates, and releases drug, excipient, and contrast agent particles into the gastric fluid. The drug particles then dissolve. But because the mass of drug in the dosage form per unit volume of gastric fluid, $M_{d,0}/V_{gf} \gg c_{s,gf}$, the drug particles do not dissolve entirely, and are carried out of the stomach with the gastric fluid flow.

Assuming that (a) the volumetric inflow and outflow rates of gastric fluid, Q_{gf}, are the same and time-invariant, (b) the particles in the stomach are perfectly mixed with the gastric fluid, and (c) no drug particle will dissolve completely so that the number of drug particles is conserved, the time to reduce the number of particles to 37 percent of the initial value may be written as:[27]

$$t_{r,p} = \frac{V_{gf}}{Q_{gf}} \quad \text{(A1)}$$

where V_{gf} is the volume of gastric fluid.

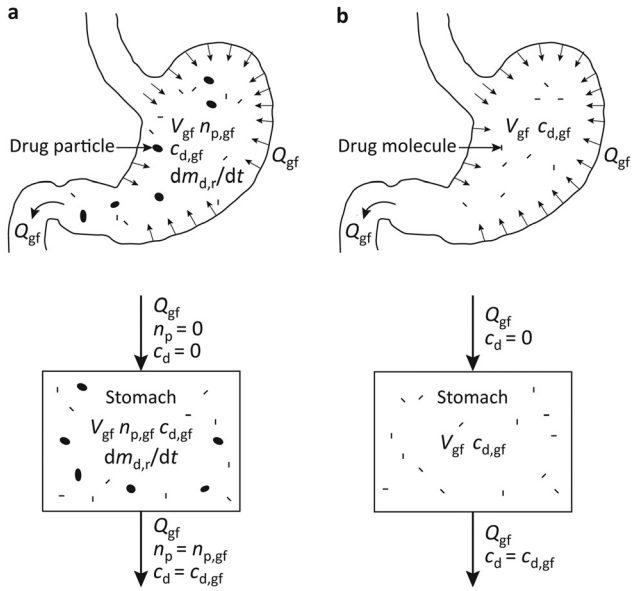

Fig. 15 Schematic of mass flow rates into and out of the stomach after administering particulate dosage forms: (a) $t < t_{r,p}$ and (b) $t \gg t_{r,p}$. Here $t_{r,p}$ is the residence time of drug particles in the stomach. The schematic is reproduced from ref. 27.

In the fasted stomach of a dog, the gastric fluid volume, V_{gf} = 20 ml, and the volumetric flow rate of gastric fluid into and out of the stomach, Q_{gf} = 14 ml h^{-1}, Appendix B. Thus, by eqn (A1) the calculated "gastric residence time" of drug particles, $t_{r,p}$ = 1.43 h. This is about the same as the measured residence time of the (comparable) contrast agent particles, 1–1.5 h.

A.4. Drug concentration in gastric fluid. Assuming that no drug is absorbed through the gastric wall, as detailed in Fig. 15 by mass balance the rate of change of the molecular concentration of drug in the gastric fluid may be written as:[27]

$$V_{gf}\frac{dc_{d,gf}}{dt} = -Q_{gf}c_{d,gf} + \frac{dm_{d,r}}{dt} \quad (A2)$$

where $dm_{d,r}/dt$ is the drug release rate by the drug particles into the gastric fluid.

From prior work, $dm_{d,r}/dt \sim M_{d,0}(c_{s,gf} - c_{d,gf})/R_{p,0}^{5/3}$ where $M_{d,0}$ is the mass of drug in the dosage form, $c_{s,gf}$ the drug solubility in the gastric fluid, and $R_{p,0}$ the radius of the drug particles. Because the particles are small and the mass of drug in the dosage form per unit volume of gastric fluid, $M_{d,0}/V_{gf} \gg c_{s,gf}$, $c_{d,gf}$ reaches $c_{s,gf}$ rapidly.

Further assuming that the drug particles remain in the stomach up to $t = t_{r,p}$, and then are flushed out immediately,[27] the drug concentration in gastric fluid may be written as:

(a) $0 \le t \le t_{r,p}$. Up to $t = t_{r,p}$,[27]

$$c_{d,gf} = c_{s,gf} \quad (A3)$$

(b) $t > t_{r,p}$. After the "residence time" of the drug particles, analogous to eqn (16),[27]

$$c_{d,gf} = c_{d,gf}\big|_{t=t_{r,p}} \exp\left(-\frac{Q_{gf}(t - t_{r,p})}{V_{gf}}\right) \quad (A4)$$

where $c_{d,gf}\big|_{t=t_{r,p}} = c_{s,gf}$, eqn (A3).

Fig. 16a plots eqn (A3) and (A4) for the relevant parameters. Up to the "residence time" of the drug particles the concentration of drug molecules in the gastric fluid is at solubility. After the "residence time" the concentration drops exponentially at the time constant, $\tau_{gf} = V_{gf}/Q_{gf}$ = 1.43 h.

A.5. Drug concentration in blood. Fig. 16b plots the measured drug concentration in blood plasma *versus* time after administering the particulate dosage forms. After an initial delay of about 30 minutes, the drug concentration increased steeply and at roughly constant rate to a peak of 0.68 μg ml^{-1} by 2.5 hours. The concentration then decreased exponentially, to 0.16 μg ml^{-1} by 6 hours and 0.026 μg ml^{-1} by 12 hours.

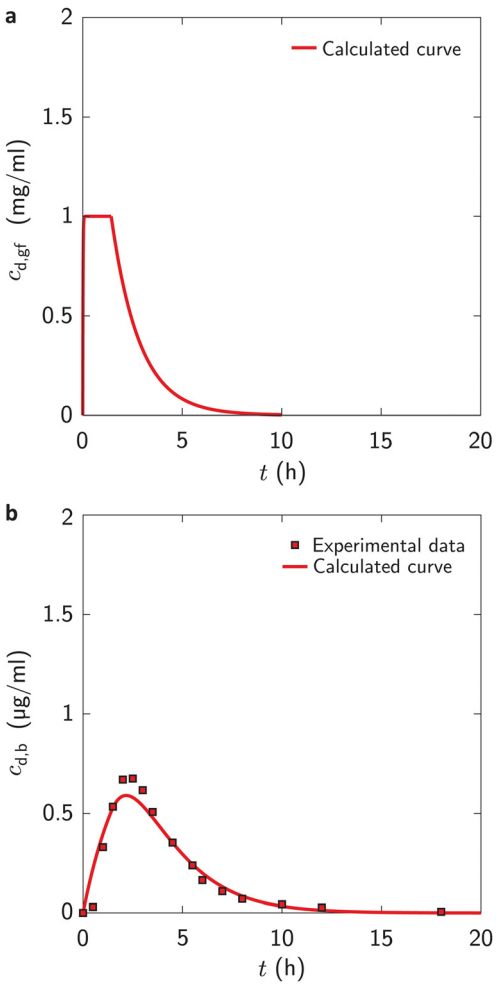

Fig. 16 (a) Molecular concentration of drug in the gastric fluid, $c_{d,gf}$, *versus* time after administering a particulate dosage form. The drug concentration is calculated by eqn (A3) and (A4) using the parameter values of Appendix B. The graph is reproduced from ref. 27. (b) Measured and calculated drug concentrations in blood *versus* time after administering particulate dosage forms. The measured values represent the average drug concentration in blood plasma of four particulate dosage forms. The calculated values are drug concentrations in blood from eqn (A5) and (A6) using the parameter values of Appendix B. The graph is reproduced from ref. 28.

In prior work, under the highly approximate assumptions that (a) all drug molecules that are released into the stomach pass into the duodenum and are absorbed by the blood stream, (b) drug distribution through the blood and tissues is fast, and (c) the drug is eliminated from the blood at a rate proportional to the drug concentration in blood, the following equations were derived for the drug concentration blood.[27]

(a) $0 \le t \le t_{r,p}$. Up to $t_{r,p}$, for $c_{d,b} = 0$ at $t = 0$,[27]

$$c_{d,b} = \frac{Q_{gf} c_{s,gf} \tau_{el}}{V_b + K_{p,t} V_t} \left(1 - \exp\left(-\frac{t}{\tau_{el}}\right)\right) \tag{A5}$$

where τ_{el} is the time constant by which drug is eliminated from the blood, V_b the volume of blood, $K_{p,t}$ the tissue-blood partition coefficient of the drug, and V_t the volume of tissue.

Eqn (A5) is also plotted in Fig. 16b for the relevant parameter values listed in Appendix B (Q_{gf} = 14 ml h^{-1}, $c_{s,gf}$ = 1 mg ml^{-1}, τ_{el} = 1.96 h, V_b = 1.1 l, $K_{p,t}$ = 2.08, and V_t = 12.8 l). The agreement between data and model is fairly good.

(b) $t > t_{r,p}$. After the "residence time" of the particles,[27]

$$c_{d,b} = \frac{Q_{gf} c_{s,gf} \tau_{el}}{V_b + K_{p,t} V_t} \times \left(\frac{\tau_{el}}{\tau_{el} - \tau_{gf}} \exp\left(-\frac{t - t_{r,p}}{\tau_{el}}\right) - \frac{\tau_{gf}}{\tau_{el} - \tau_{gf}} \exp\left(-\frac{t - t_{r,p}}{\tau_{gf}}\right) - \exp\left(-\frac{t}{\tau_{el}}\right)\right) \tag{A6}$$

where $c_{d,b}\big|_{t=t_{r,p}}$ may be obtained from eqn (A5).

Fig. 16b further plots eqn (A6) for Q_{gf} = 14 ml h^{-1}, $c_{s,gf}$ = 1 mg ml^{-1}, τ_{el} = 1.96 h, V_b = 1.1 l, $K_{p,t}$ = 2.08, V_t = 12.8 l, and τ_{gf} = $t_{r,p}$ = 1.43 h. Because $\tau_{el} > \tau_{gf}$, the drug concentration in blood drops exponentially at the time constant, τ_{el} = 1.96 h. Again, the model and data agree.

B: Parameters and properties

Symbol	Description	Value	Ref.
c_b	Concentration of water at fiber–fluid interface	1000 kg m^{-3} [a]	—
$D_{d,df}$	Drug diffusivity through expanded dosage form	4.22×10^{-10} m^2 s^{-1} [b]	25
D_w	Diffusivity of water or gastric fluid in fiber	4.1×10^{-12} m^2 s^{-1}	From section 3.3
H	Thickness of expanded fibrous dosage form	9.8 mm[c]	—
H_0	Thickness of solid fibrous dosage form	6.5 mm	From Table 1
$K_{p,t}$	Tissue-blood partition coefficient	2.08	28
$M_{d,0}$	Drug mass in solid dosage forms	200 mg	—
Q_{gf}	Flow of gastric fluid into the intestines	14 ml h^{-1}	28
$R_{f,0}$	Radius of solid fibers	149 μm	From Table 1
Δt	Time increment between integer indexes in numerical calculations	0.1 h	—
V_b	Volume of blood	1.1 l[d]	28
V_{gf}	Volume of gastric fluid in fasted stomach	20 ml	28
V_t	Volume of organs and tissues	12.8 l[d]	28
λ_0	Inter-fiber spacing in solid fibrous dosage form	601 μm	From Table 1
ρ_w	Density of water	1000 kg m^{-3}	—
τ_{el}	Time constant of the process by which drug is eliminated from the blood	1.96 h[e]	28
φ_f	Volume fraction of fibers in solid fibrous dosage form	0.57	From Table 1

[a] Assumed to be the same as the density of water, ρ_w. [b] Assumed to be the same as the diffusivity of drug in the dissolution fluid. In ref. 25 the diffusivity of drug molecules in the dissolution fluid (acidic water), $D_{d,fl}$, was estimated by an adapted form of the Stokes–Einstein equation: $D_{d,fl} = k_b T/6\pi r_d \mu_{fl}$, where k_b is Boltzmann's constant, T the temperature, r_d the radius of a drug molecule, and μ_{fl} the viscosity of the dissolution fluid. The radius of a drug molecule was approximated as $r_d = (3M_{w,d}/4\pi N_A \rho_d)^{1/3}$ where $M_{w,d}$ is the molecular weight of the drug, N_A Avogadro's number, and ρ_d the density of the solid drug. For the parameters of this work, $M_{w,d}$ = 0.53 kg mol^{-1}, ρ_d = 1360 kg m^{-3}, T = 310 K, and μ_{fl} = 0.001 Pa s, the diffusivity, $D_{d,fl} = 4.22 \times 10^{-10}$ m^2 s^{-1}. [c] In agreement with the results shown in Fig. 5, the dimensions of the expanded dosage form are about 1.5 times the dimensions of the solid dosage form. Thus, $H = 1.5 \times H_0$, where H_0 = 6.5 mm. [d] From prior work,[28] reasonable estimates of the volume of blood and tissue of beagle dogs of size and weight used in this study are 1.1 and 12.8 l, respectively. [e] From prior work,[27,28] if the drug is eliminated in the liver by Fickian diffusion from the sinusoidal blood capillaries across the hepatic plates into the bile, $\tau_{el} = (V_b + K_{p,t}V_t)\ln(R_o/R_i)Q_{b,s}/2\pi K_{p,hp} D_{d,hp} L_s Q_{b,l}$, where R_o is the outer radius of the annulus of hepatic plate surrounding a sinusoid, R_i the radius of a sinusoidal capillary, $Q_{b,s}$ the flow rate of blood through a sinusoid, $K_{p,hp}$ the partition coefficient of drug between a sinusoidal capillary and hepatic plates, $D_{d,hp}$ the drug diffusivity through hepatic plates, L_s the length of a sinusoid, and $Q_{b,l}$ the flow rate of blood through the portal vein into the liver. From prior work, R_o = 15 μm, R_i = 5 μm, $K_{p,hp}$ = 2.08, $D_{d,hp} = 5.24 \times 10^{-12}$ m^2 s^{-1}, L_s = 275 μm, and $Q_{b,l}$ = 9 ml s^{-1}.

C: Data of drug concentration in blood plasma after administering the fibrous dosage forms to the dogs

Experiment 1 (dog 1)		Experiment 2 (dog 2)	
t (h)	$c_{d,b}$ (μg ml^{-1})	t (h)	$c_{d,b}$ (μg ml^{-1})
0	0	0	0
0.5	0.05	0.5	0.05
1	0.086	1	0.168
1.5	0.419	1.5	0.618
2	1.241	2	0.934
2.5	1.699	2.5	1.26
3	2.09	3	1.296
4	2.242	4	1.406
4.5	2.227	4.5	1.147
5	2.034	5	1.037
6	1.782	6	0.612
6.5	1.346	6.5	0.567
7	1.302	7	0.452
7.5	0.984	7.5	0.38
8	0.945	8	0.317
8.5	0.86	8.5	0.269
9	0.705	9	0.168
9.5	0.671	9.5	0.154
10	0.612	10	0.111
10.5	0.616	10.5	0.081
11	0.521	11	0.057
11.5	0.448	11.5	0.05
12	0.423	12	0
13	0.3	13	0
14	0.257	14	0
15	0.199	15	0
16	0.174	16	0
17	0.128	17	0
18	0.095	18	0

Acknowledgements

Prof. Giovanni Terrasi, Mr Silvain Michel and Mr Cyrill Schmid of Empa Dübendorf, Switzerland, are acknowledged for providing access to the DSC testing facilities at Empa Dübendorf. Dr Thomas Echtermann and Dr Nadja Aeberhard of the Vetsuisse Faculty, University of Zurich, are acknowledged for assistance with *in vivo* studies. Mr Fabian Weber of Polarwind AG in Zurich, Switzerland, is acknowledged for photographing the dosage forms shown on the cover image. This project received financial support from Enzian Pharmaceutics and the innovation agency of the government of Switzerland (Innosuisse).

References

1 G. L. Amidon, H. Lennernäs, V. P. Shah and J. R. Crison, A theoretical basis for a biopharmaceutic drug classification: The correlation of *in vitro* drug product dissolution and *in vivo* bioavailability, *Pharm. Res.*, 1995, **12**, 413–420.
2 C. A. Lipinski, Drug-like properties and the causes of poor solubility and poor permeability, *J. Pharmacol. Toxicol. Methods*, 2000, **44**, 235–249.
3 I. L. O. Buxton and L. Z. Benet, in *Goodman & Gilman's the pharmacological basis of therapeutics*, ed. L. L. Brunton, B. Chabner and B. C. Knollmann, McGraw Hill, New York, NY, 12th edn, 2011, ch. 2, pp. 17–39.
4 N. R. Budha, A. Frymoyer, G. S. Smelick, J. Y. Jin, M. R. Yago, M. J. Dresser, S. N. Holden, L. Z. Benet and J. A. Ware, Drug Absorption Interactions Between Oral Targeted Anticancer Agents and PPIs: Is pH-Dependent Solubility the Achilles Heel of Targeted Therapy?, *Clin. Pharmacol. Ther.*, 2012, **92**, 203–213.
5 M. Ashford, in *Aulton's Pharmaceutics: The design and manufacture of medicines*, ed. M. E. Aulton and K. M. G. Taylor, Elsevier, London, UK, 5th edn, 2018, Part 4, ch. 20, pp. 319–338.
6 J. Siepmann and F. Siepmann, Mathematical modeling of drug dissolution, *Int. J. Pharm.*, 2013, **453**, 12–24.
7 S. Yassin, D. J. Goodwin, A. Anderson, J. Sibik, D. I. Wilson, L. F. Gladden and J. A. Zeitler, The disintegration process in microcrystalline cellulose based tablets, part 1: influence of temperature, porosity and superdisintegrants, *J. Pharm. Sci.*, 2015, **104**, 3440–3450.
8 A. T. M. Serajuddin, Salt formation to improve drug solubility, *Adv. Drug Delivery Rev.*, 2007, **59**, 603–616.
9 S. Sarkar, A. P. Roy, S. Mitra, G. Nandi, R. Sahu, T. K. Dua and P. Paul, Preparation and characterization of efavirenz cocrystal-encapsulated pronanoliposomes for antiretroviral therapy with improved bioavailability, *RSC Pharm.*, 2025, **2**, 342–352.
10 B. C. Hancock and G. Zografi, Characteristics and significance of the amorphous state in pharmaceutical systems, *J. Pharm. Sci.*, 1997, **86**, 1–12.
11 B. C. Hancock and M. Parks, What is the true solubility advantage for amorphous pharmaceuticals?, *Pharm. Res.*, 2000, **17**, 397–404.
12 B. C. Hancock, Disordered drug delivery: destiny, dynamics and the Deborah number, *J. Pharm. Pharmacol.*, 2002, **54**, 737–746.
13 M. Pudipeddi and A. T. M. Serajuddin, Trends in solubility of polymorphs, *J. Pharm. Sci.*, 2005, **94**, 929–939.
14 A. Parkes, E. Spoletti, J. O'Reilly, M. Lusi, A. Ziaee and E. O'Reilly, Controlled isolation of a novel polymorphic form of chlorothiazide by spray drying, *RSC Pharm.*, 2025, **2**, 398–412.
15 W. L. Ciou and S. Riegelman, Pharmaceutical applications of solid dispersion systems, *J. Pharm. Sci.*, 1971, **60**, 1281–1302.
16 A. T. M. Serajuddin, Solid dispersion of poorly water-soluble drugs: early promises, subsequent problems, and recent breakthroughs, *J. Pharm. Sci.*, 1999, **88**, 1058–1066.
17 H. Joshi, R. Tejwani, M. Davidovich, V. P. Sahasrabudhe, M. Jemal, M. S. Bathala, S. A. Varia and A. T. M. Serajuddin, Bioavailability enhancement of a poorly water-soluble drug by solid dispersion in polyethylene glycol-polysorbate 80 mixture, *Int. J. Pharm.*, 2004, **269**, 251–258.

18 D. E. Alonzo, G. G. Z. Zhang, D. Zhou, Y. Gao and L. S. Taylor, Understanding the behavior of amorphous pharmaceutical systems during dissolution, *Pharm. Res.*, 2010, **27**, 608–618.
19 G. A. Ilevbare, H. Liu, K. J. Edgar and L. S. Taylor, Understanding polymer properties important for crystal growth inhibition-impact of chemically diverse polymers on solution crystal growth of ritonavir, *Cryst. Growth Des.*, 2012, **12**, 3133–3143.
20 B. R. de Alvarenga Jr. and L. S. Taylor, Release performance and crystallization of racemic and enantiopure praziquantel amorphous solid dispersion in various media, *RSC Pharm.*, 2025, **2**, 1125–1138.
21 A. H. Blaesi and N. Saka, Expandable fibrous dosage forms for prolonged drug delivery, *Mater. Sci. Eng., C*, 2021, **120**, 110144.
22 A. H. Blaesi and N. Saka, Expandable, dual-excipient fibrous dosage forms for prolonged delivery of sparingly soluble drugs, *Int. J. Pharm.*, 2022, **615**, 120396.
23 A. H. Blaesi, D. Kümmerlen, H. Richter and N. Saka, Mechanical strength and gastric residence time of expandable fibrous dosage forms, *Int. J. Pharm.*, 2022, **613**, 120792.
24 A. H. Blaesi, T. Echtermann, H. Richter and N. Saka, The effect of a semi-permeable, strengthening fiber coating on the expansion, mechanical properties, and residence time of gastroretentive fibrous dosage forms, *Int. J. Pharm.*, 2023, **642**, 122378.
25 A. H. Blaesi and N. Saka, Gastroretentive fibrous dosage forms for prolonged delivery of sparingly-soluble tyrosine kinase inhibitors. Part 1: Dosage form design, and theoretical models of expansion, mechanical strength, and drug release, *Int. J. Pharm.*, 2025, **674**, 124360.
26 A. H. Blaesi and N. Saka, Gastroretentive fibrous dosage forms for prolonged delivery of sparingly-soluble tyrosine kinase inhibitors. Part 2: Experimental validation of the models of expansion, mechanical strength, and drug release, *Int. J. Pharm.*, 2025, **674**, 124361.
27 A. H. Blaesi and N. Saka, Gastroretentive fibrous dosage forms for prolonged delivery of sparingly-soluble tyrosine kinase inhibitors. Part 3: Theoretical models of drug concentration in blood, *Int. J. Pharm.*, 2025, **674**, 124362.
28 A. H. Blaesi, H. Richter and N. Saka, Gastroretentive fibrous dosage forms for prolonged delivery of sparingly-soluble tyrosine kinase inhibitors. Part 4: Experimental validation of the models of drug concentration in blood, *Int. J. Pharm.*, 2025, **674**, 124363.
29 A. H. Blaesi and N. Saka, 3D-micro-patterned fibrous dosage forms for immediate drug release, *Mater. Sci. Eng., C*, 2018, **84**, 218–229.
30 A. H. Blaesi and N. Saka, Fibrous dosage forms by wet 3D-micro-patterning: Process design, manufacture, and drug release rate, *Eur. J. Pharm. Biopharm.*, 2018, **130**, 345–358.
31 J. Crank, *The Mathematics of Diffusion*, Oxford University Press, Oxford, UK, 2nd edn, 1975, pp. 47–49.
32 M. Herbrink, H. Vromans, J. Schellens, J. Beijnen and B. Nuijen, Thermal stability study of crystalline and novel spray-dried amorphous nilotinib hydrochloride, *J. Pharm. Biomed. Anal.*, 2018, **148**, 182–188.